ORIGINAL ARTICLE

Reconstruction of Low-Quality Channel Data in Magnetoencephalography using Surface Reconstruction and Interpolation Methods

Hanie Arabian [1], Alireza Karimian [1*], Hamid Reza Marateb [1,2], Carolina Migliorelli [3], Miquel Angel Mañanas [2,4], Sergio Romero [2,5], Antonio Russi [6], Rafał Nowak [7]

[1] *Department of Biomedical Engineering, Faculty of Engineering, University of Isfahan, Isfahan, Iran*

[2] *Department of Automatic Control, Biomedical Engineering Research Center, Polytechnic University of Catalonia, BarcelonaTech (UPC), Barcelona, Spain*

[3] *Unit of Digital Health, Eurecat, Centre Tecnològic de Catalunya, 08005 Barcelona, Spain*

[4] *Networking Center in Bioengineering, Biomaterials, and Nanomedicine (CIBER-BBN), Barcelona, Spain*

[5] *CIBER de Bioingeniería, Biomateriales y Nanomedicina (CIBER-BBN), Madrid, Spain*

[6] *Epilepsy Unit, Hospital Quirón Teknon, Barcelona, Spain*

[7] *Magnetoencephalography Unit, Hospital Quirón Teknon, Barcelona, Spain*

*Corresponding Author: Alireza Karimian

Email: karimian@eng.ui.ac.ir

Received: 13 April 2025 / Accepted: 18 August 2025

Abstract

Purpose: Magnetoencephalography (MEG) is a brain imaging method with high temporal and acceptable spatial resolution, achieved by recording neural magnetic fields. The data quality of this imaging method is compromised due to reasons such as the failure of one or more sensors. This study aims to explore the efficiency of the various data reconstruction techniques in MEG for recovering poor-quality or missing channel data.

Materials and Methods: We compared three surface reconstruction methods (Mean, Median, and Trimmed mean), two partial differential equations (modified Poisson and Diffusion equation), and a Finite Element-based interpolation method using data from 11 young adults (aged 30±12). Using varying levels of simulated data loss (2%, 5%, 11%, and 16%), we assessed each method in terms of time taken for reconstruction, R-squared, root mean squared error (RMSE), and signal-to-noise ratio (SNR) compared to a reference signal. Statistical tests (P-value < 0.05) were used to analyze the relationships between the mentioned evaluation criteria. Generalized Linear Models revealed that surface reconstruction methods and finite-element interpolation outperformed partial differential equations.

Results: The Trimmed mean method achieved the highest R-squared (0.882 ± 0.0610) and lowest RMSE (0.0155 ± 0.00904) with a reconstruction time of 9.5154 microseconds for a 500-millisecond epoch of MEG channel data.

Conclusion: The surface reconstruction methods can recover the noisy or lost signal in MEG with a suitable error and required time. These findings support the use of robust statistical strategies for improving MEG signal quality, especially in high-density sensor arrays.

Keywords: Data Reconstruction; Finite Element Interpolation; Image Inpainting; Magnetoencephalography; Signal Enhancement; Surface Reconstruction.

Copyright © 2026 Tehran University of Medical Sciences.
This work is licensed under a Creative Commons Attribution-NonCommercial 4.0 International license (https://creativecommons.org/licenses/by-nc/4.0/). Noncommercial uses of the work are permitted, provided the original work is properly cited.
DOI: https://doi.org/10.18502/fbt.v13i3.22733

1. Introduction

Magnetoencephalography (MEG) is a non-invasive neuroimaging technique that captures the weak magnetic fields generated by synchronized neuronal currents [1-3]. Although functional MRI (fMRI) offers superior spatial resolution, it lacks the temporal fidelity required to capture real-time brain activity [4, 5]. MEG provides high temporal resolution and non-invasive access to neuronal activity, making it particularly suited for capturing fast cortical dynamics [6-10]. Studying brain function is vital due to its useful latent information regarding the diagnosis and treatment of certain diseases such as Obsessive-Compulsive Disorder (OCD) [11], epilepsy [12], Alzheimer's [13], and psychiatric disorders [14, 15].

MEG signals contain information about the brain's active neural sources and their interactions [16, 17]. Inverse reconstruction of neural sources leads to the detection of interactions between different brain areas [18, 19]. While MEG provides high-quality recordings, it faces challenges related to data quality. One limitation is the presence of low-quality or corrupted channel data, which can occur due to sensor noise, movement artifacts, or other technical issues. These corrupted channels can significantly impact the accuracy of source reconstruction, limiting our ability to understand brain activity and connectivity [19-21]. Prior efforts in MEG artifact correction have focused on source localization accuracy or component-level cleaning using techniques such as Signal-Space Projection (SSP) [22], Independent Component Analysis (ICA) [23], minimum norm estimation [24], and, more recently, the integration of fMRI data for improved source reconstruction [25]. However, fewer studies have evaluated sensor-level interpolation performance under simulated dropout. In addition, these methods typically ignore or discard low-quality channels in the signal pre-processing phase, leading to a loss of valuable information [20].

In 2006, Sekihara *et al.* introduced the Beamformer method, which used the covariance matrix calculation to eliminate the effect of background brain activity interference in the inverse reconstruction of neural resources [26]. In 2007, Brooks *et al.* introduced the Dual-Core Beamformer (DCBF) method to overcome the limitation of the Beamformer method in the face of source correlation. They reconstructed the correlated sources by using spatial domain filters set from the linear combination of the vectors of both possible dipole neural sources [27]. In 2008, Cheveigne and Simon proposed the Sensor Noise Suppression (SNS) method for reconstructing channel data information, in which the specific noises of each sensor were replaced by the regression of noisy data from adjacent sensors [28]. In 2014, Lina *et al.* introduced the Wavelet-based localization method to reconstruct brain oscillations to locate the signal generation, in which the signal was examined in the time-frequency domain [3]. In 2015, Fukushima *et al.* introduced the Multivariate Autoregressive (MAR) method for reconstructing MEG signal data to examine the direct interactions of different brain regions based on regression coefficients [29]. In 2016, Cheveigne introduced the Sparse Time Artifact Removal (STAR) algorithm to detect and eliminate specific noises, such as sensor noise, that did not propagate in time and space. The noise-infected part was corrected by determining the correlation coefficient of the noise-free data by the covariance matrix [30]. In 2018, Wang *et al.* introduced a method to correct artificial interactions caused directly by mixing and spurious interactions in functional connectivity analyses using bundling observed functional connections into hyperedges by their adjacency in signal mixing [1]. In 2021, Suzuki and Yamashita demonstrated the use of meta-analysis fMRI data to overcome the problem of the lower number of sensors than neural sources to improve current source reconstruction in MEG; however, it boosted the cost of measurement and the burden on subjects [25]. The limitations of these methods, including sensitivity to correlated sources, high computational cost, and potential loss of spatial resolution, are summarized in Table 1.

Although most previous methods have focused on source estimation, the reconstruction problem at the channel level has been less studied. In many MEG signal processing studies, low-quality or noisy channels are removed to maintain the accuracy of the analysis. However, removing channels may impact the spatial resolution of neural activity mapping and introduce biases in subsequent analyses.

This work builds upon our previous study [31], but extends it in several important ways. First, in addition to the Mean, Median, and Finite Element interpolation

Table 1. Previous approaches related to MEG signal cleaning and reconstruction

Author-Date	Brief description	Limitations
Sekihara, 2006	Eliminating the effect of interferences caused by spontaneous brain activities by using its covariance matrix and computing the resources' current density by weighting all channels at each moment.	Requires control-state measurements for background interference covariance. Background interference can blur reconstruction results significantly.
Brooks, 2007	Reconstruction of the correlated sources by spatial domain filters, which were set from the linear combination of the vectors of both possible dipole neural sources.	High Computational complexity.
Cheveigne, 2008	Removing any uncorrelated sensor noise by calculating the correlation coefficient of the recorded channels' signal of each source.	It cannot remove correlated noises. Elimination of uncorrelated brain signals.
Lina, 2014	Reconstruction of oscillatory brain activities by examining low-density channels' signal in the time-frequency domain and localization of event-related potentials.	To reconstruct event-related potential (ERP) only.
Fukushima, 2015	Examining the interactions of different brain areas by examining the spatial patterns of brain activities in the MRI image by calculating the regression coefficients of the MEG channels.	For linear sources only. Not able to examine long-term interactions.
Cheveigne, 2016	Identifying and removing channel-characteristic noises that are not spread in time and space and correcting them by imaging the noise part on a subset of other channels.	It cannot remove common channel noise.
Wang, 2018	Correcting spurious interactions in functional connections analyses using source-reconstructed MEG/EEG[1] data.	Signal mixing source leakage remains a significant confounder for network localization.
Suzuki, 2021	Using meta-analysis fMRI[2] data in current source reconstruction instead of individual fMRI data.	High computational cost proportional to the number of candidates.

[1] Electroencephalography (EEG)
[2] functional Magnetic Resonance Imaging (fMRI)

methods evaluated previously, the current study systematically examines the Trimmed Mean method and compares it with six algorithms, including two PDE-based approaches (modified Poisson and Diffusion equations). Second, we introduce a Generalized Linear Model (GLM) framework for statistical comparison across multiple corruption levels (2%, 5%, 11%, and 16%) and assess associations between R-squared, RMSE, and SNR. Third, while the earlier study focused on descriptive comparisons, the present work includes repeated trials with randomized corruption patterns to evaluate robustness under variable data loss scenarios. Finally, a correlation-based neighbor selection strategy is implemented to mitigate the influence of corrupted neighboring channels, which was not addressed in the earlier study. These additions provide a more comprehensive and statistically rigorous evaluation of MEG channel reconstruction techniques. These methodological advances and the expanded evaluation

framework clearly differentiate this work from our previous study [31] and provide novel insights into the robustness of MEG reconstruction methods.

2. Materials and Methods

This section describes the procedures for simulating signal corruption in MEG data and evaluating reconstruction quality using statistical metrics such as SNR and R-square, without performing neural source localization. The choice of SNR and R-squared as evaluation metrics was based on their relevance in assessing the similarity between reconstructed and original signals. SNR provides a measure of signal quality, while R-squared quantifies the proportion of variance explained by the reconstructed signal. A flowchart is shown in Figure 1 to indicate the sequence of steps to facilitate the understanding of the entire implementation process in this study. Then, each step is explained in the following sub-sections with the necessary details.

2.1. Data Acquisition

In this research, a study was performed on MEG signals of eleven young adults (aged 30±12) with no history of brain disorders at Barcelona Children's Hospital and made available through a joint project with them. These signals were recorded in a magnetically shielded room with a whole-head 148-channel magnetometer device at a sampling frequency of 678.17 Hz called 4D-Neuroimaging (BTi San Diego, California, USA). MEG signal measurement was performed continuously for ten minutes in a resting state with closed eyes. The subjects were placed in the supine position to reduce the head movement effect [32].

The sensors were located at a distance from the head and with an average distance of about 2.5 cm from each other on a helmet. The position and orientation of each sensor were measured relative to the center of the subject's head. Before each measurement, the shape of the patient's head and its landmarks, such as left and right ears, were digitized with 3Space Fasttrack (Polhemus, Vermont, USA). To determine the head position, a right-handed coordinate system called the head-frame coordinate system was used in which the x-axis was to the front, the y-axis was to the left, and the z-axis was to the top of the head. The position of magnetometers could be obtained by the Brainstorm software [33].

2.2. Preprocessing

In the signal recording path, a high-pass filter with a cut-off frequency of 1 Hz was used before the data was digitized. After the recording process was complete, cardiac artifacts of the signals were filtered using automatic blind source separation algorithms using the Fieldtrip toolbox in MATLAB [34]. In the next step of preprocessing of the MEG signal, Infinite Impulse Response (IIR) filters were used due to their computational efficiency, despite their nonlinear phase characteristics [20]. The acceptable frequency range of this signal is [1-90] Hz; Therefore, to remove its useless components, a 6th-degree Butterworth band-pass filter with a bandwidth of [1-90] Hz was used, and to remove the power-line noise, a 4th degree

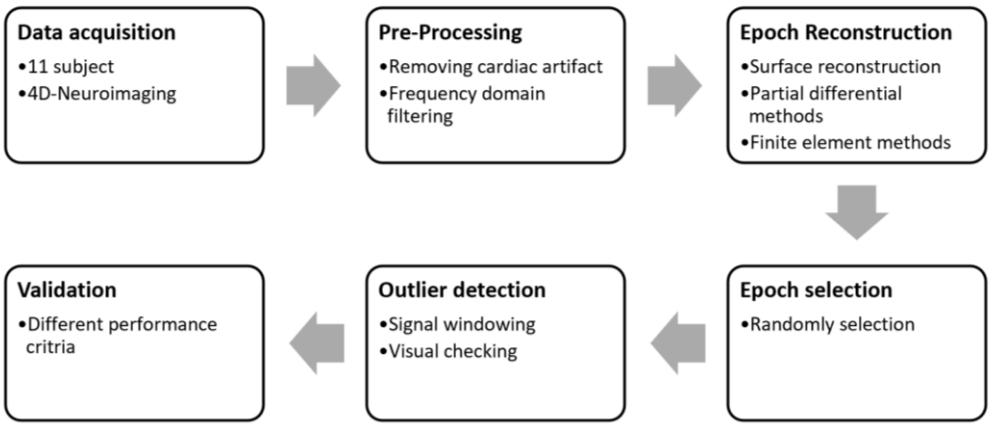


Figure 1. Overview of the study workflow for MEG channel reconstruction evaluation

Butterworth band-stop filter with a bandwidth of [48-52] Hz was used [35].

2.3. Epoch Selection

After dividing each channel's data into 500-millisecond epochs, some had to be considered outliers and reconstructed using their neighboring data. Although the initial MEG data used in this study were of high quality, signal corruption was simulated by randomly removing portions of the signal in selected channels. To ensure statistical validity, the proportion of corrupted channels was limited to less than 25% of the total. Because this study's volume of data and calculations was huge and time-consuming, four random values between 2 and 25% were selected (equal to 2, 5, 11, and 16%) as outliers. These percentages were chosen to evaluate the robustness of reconstruction methods under increasing data loss scenarios. Then, in four separate stages, where each stage was repeated 4 times, 2, 5, 11, and 16% of epochs were randomly selected and considered as corrupt epochs to ensure that the result was obtained by no chance [36, 37]. During reconstruction, only the corrupted segments were considered, and the uncorrupted parts were excluded from the reconstruction process to avoid bias. When reconstructing a corrupted channel based on its spatial neighbors, there was a possibility that some neighboring channels also contained corrupted segments due to the random nature of the dropout process. To mitigate the impact of such neighbors, we calculated the correlation between the candidate neighboring channels and the target channel. Channels with correlation values below 0.4 were excluded from the reconstruction to ensure that only informative and reliable neighbors contributed to the interpolation process. In this way, the conditions of sensor failure or noise and data loss in some channels were simulated to consider their impact on reconstruction methods.

2.4. Epoch Reconstruction

MEG data is inherently spatially correlated; that is, channels nearby in the sensor array often reflect similar underlying brain activity [38, 39]. Thus, three surface reconstruction methods were used in this study: Mean, Median, and Trimmed mean. In the Mean and Median method, each time sample in the intended epoch was reconstructed by the average and median time samples in the 13 nearest neighbors, respectively. Median could reduce the influence of outliers and is beneficial when the data may exhibit skewed distributions. Also, in the Trimmed mean method, first, the data of the 13 nearest neighbors were sorted, and then, after omitting 10% of the data (the lowest and the highest), the average of the remaining samples was calculated. Trimmed mean strikes a balance between mean and median, allowing the exclusion of extreme values while still considering a larger portion of the data than the median alone. The use of 13 neighbors, which includes all the first-ordered and some second-ordered neighbors, would strike a balance between being sufficiently comprehensive to capture local spatial correlations while avoiding excessive noise that might arise from considering too many distant sensors.

Using diffusion processes to model the spread of information and data values in space can effectively smooth out noise and recover signals based on spatial correlations, making them particularly suitable for multi-channel signal data such as MEG [40]. The Modified Diffusion and Poisson Equation have been used in this study due to their ability to effectively capture spatial correlations among neighboring data points [31, 36]. In the context of MEG data, each sensor's measurement is influenced by the activity of nearby sensors. The initial condition of the data was necessary for these equations; therefore, since the sensors were located on the surface of the head, differentiation was possible only in two dimensions. Thus, a three-dimensional to two-dimensional mapping was used to locate the sensors. In this mapping, after calculating the standard deviation of the coordinates of each sensor with eight closer neighbors, the dimension with the least standard deviation was ignored, and the distance of each sensor from its neighbors was calculated according to their coordinates in the two other dimensions.

Then, the initial conditions for each intended sensor were defined by averaging the Laplace values obtained from its intact neighbors. After calculating the initial, the modified Poisson equations are used to recover the lost data [31, 36].

To calculate the modified Diffusion, the initial conditions should be applied to Equation 1 [31, 36].

$$u_{xx} + u_{yy} = IC \quad (1)$$

Where u_{xx} and u_{yy} were the second-order derivatives of the signal in the horizontal and vertical directions, respectively. IC is the calculated initial conditions in the modified Poisson section.

FEM provides a robust framework for approximating complex functions locally using piecewise polynomial functions over finite elements. In the context of your MEG data, each quadrilateral element represents a localized area around a sensor, allowing for a more refined approximation of the signal near the corrupted data. Quadrilateral elements were used to implement the FEM in this study. Thus, the four nearest neighbors of each sensor were identified [31].

2.5. Validation

After reconstructing the selected epochs, the reconstructed signal should be compared with the original signal to evaluate the performance of each method for the mentioned epochs. Hence, in addition to R-squared, RMSE, SNR, Average Nearest Neighbor (ANN), and Local Image Contrast (LIC) criteria were calculated according to Equations 2 to 6, respectively.

$$R^2(i,j) = 1 - \left(\frac{\sum_{i,j\in I}\left(u_{ij} - \tilde{u}_{ij}\right)^2}{\sum_i \left(u_{ij} - \mu_{u_{ij}}\right)^2} \right) \quad (2)$$

$$RMSE(i,j) = \sqrt{\frac{1}{S}\sum_{i,j\in I}\left(u_{ij} - \tilde{u}_{ij}\right)^2} \quad (3)$$

$$SNR(i,j) = 10Log\frac{\sum_{i,j\in I} u_{ij}^2}{\sum_{i,j\in I}\left(u_{ij} - \tilde{u}_{ij}\right)^2} \quad (4)$$

Where j and i are the epochs and channel numbers, respectively. Also, u_{ij} and $\tilde{u}_{ij}$ are the original and reconstructed time samples of epoch I with S time samples, respectively. The average of the original epoch samples is shown by $\mu_{u_{ij}}$. SNR and R-squared provide signal-level evaluations of reconstruction quality. A high SNR indicates that the reconstruction did not introduce much additional noise, and a high R-squared means that the structure of the original signal was preserved.

$$ANN = \frac{\sum_{i=1}^{n} d_i}{0.5\sqrt{n} \times A} \quad (5)$$

Where n was the number of bad epochs, A was the number of all the epochs, and d_i was the minimum distance of the bad epoch to its nearest bad neighbor epoch.

$$LIC = \frac{\sqrt{\sum_{i=1}^{n}(x_i - \mu_i)^2}}{N+1} \quad (6)$$

Where μ_i is the average of the N neighboring values of x_i and n is the number of samples in each epoch.

Besides, another evaluation criterion called the Percentage of the Outlier Border (POB) was used to examine the degree of dependence of the performance of each method on the location of outliers. Afterward, the ratio of the outliers at the borders to the total number of outliers was calculated.

2.6. Statistical Methods

2.6.1. General Approach

Pearson's correlation coefficient (r) was calculated to show the association between the following performance indices: R-squared, RMSE, and SNR. The Confidence Interval (CI) of 95% was also reported for the correlation coefficients. The study employed Generalized Linear Models (GLM) [41, 42] to compare the effectiveness of various methods in reconstructing MEG signals from corrupted channels and their dependence on several factors.

2.6.2. GLM Specifications

Model Fit: GLM was used to analyze the performance of each method under varying conditions of missing rates, LIC, ANN, and POB. The goodness-of-fit measure R-squared was used as the performance index.

Significance Testing: P-values were calculated to determine the statistical significance of differences in performance among methods. Mean±std were reported for the continuous variables. P-values less than 0.05 were considered significant. Software and Package: Analyses were conducted using R software [43] (version 4.3.2) with the "glm2" package [44].

The performance of each reconstruction method was evaluated in terms of the processing time required to implement each method on a 64-bit Laptop with an Intel 7-core processor clocked at 2.6 GHz and 12 GB of RAM. All the algorithms mentioned were programmed in MATLAB 2016a (The MathWorks, Inc., Natick, Massachusetts, United States).

3. Results

Figure 2 provides a qualitative comparison of the reconstructed signals for a representative corrupted epoch using the six evaluated methods. The original signal (solid black) is plotted alongside the reconstructed signal in each subplot. This visual comparison highlights the accuracy and fidelity of different reconstruction approaches under a typical dropout scenario. Visual proximity of the reconstructed signal to the original signal indicates higher reconstruction accuracy.

To assess the statistical significance of reconstruction methods under varying corruption rates, a Generalized Linear Model (GLM) was applied. Fixed effects included method type (6 levels) and corruption rate (4 levels), while the dependent variable was R-squared. Post-hoc comparisons with Bonferroni correction revealed that Trimmed Mean consistently outperformed other methods across all corruption levels ($p < 0.001$), particularly at 11% and 16% dropout conditions.

Table 2 reports the mean ± standard deviation of R-squared, RMSE, and SNR values for each reconstruction method, averaged over four repeated runs at dropout rates of 2%, 5%, 11%, and 16%. The correlation coefficient between R-squared and RMSE was -0.75 [CI 95%: -0.744, -0.745] (P<0.001). The association between R-squared and SNR was 0.22 [CI 95%: 0.220,0.221] (P<0.001). Such an association between RMSE and SNR was -0.60 [CI 95%: -0.603, -0.603] (P<0.001). The R-squared was used as the performance index in the statistical analyses due to its significant association with SNR and RMSE.

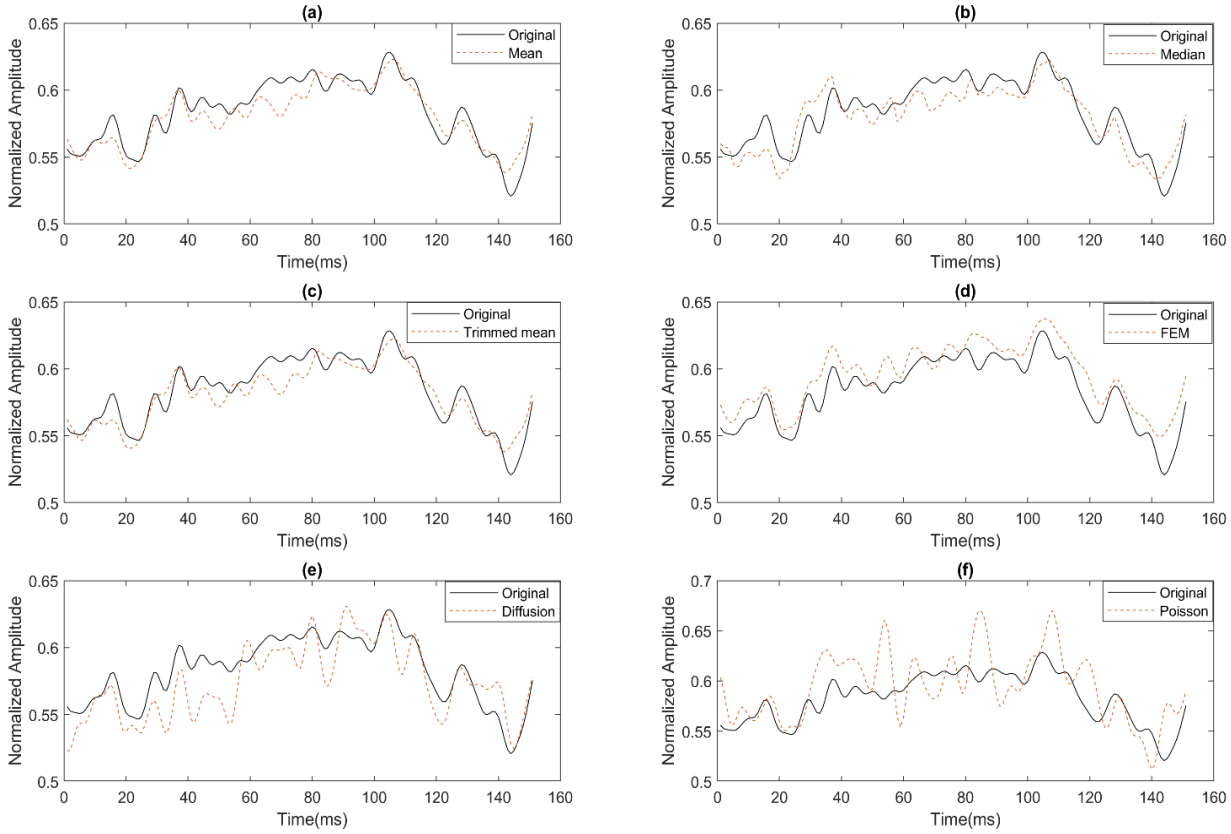


Figure 2. Comparison of the original and the reconstructed signal. The solid black curve in diagrams (a) to (d) represents the original signal. The dotted line curve in diagrams (a) to (d) shows the reconstructed signal by Mean, Median, Trimmed mean, FEM, Modified diffusion equation, and Modified Poisson equation methods, respectively

Table 2. The performance of different reconstruction methods

Method	SNR		RMSE		R-squared	
	Mean (std)	Median [Min, Max]	Mean (std)	Median [Min, Max]	Mean (std)	Median [Min, Max]
Mean	0.870 (0.0772)	0.884 [-2.11, 0.995]	0.0159 (0.00888)	0.0135 [0.00411, 0.274]	33.5 (3.96)	33.9 [10.1, 44.5]
Median	0.877 (0.0532)	0.884 [0.474, 0.994]	0.0160 (0.00949)	0.0133 [0.00386, 0.309]	33.5 (4.11)	34.0 [9.09, 45.0]
Trimmed mean	0.882 (0.0611)	0.892 [-1.20, 0.994]	0.0155 (0.00904)	0.0129 [0.00411, 0.294]	33.8 (4.09)	34.3 [9.51, 44.4]
Finite Element Method (FEM)	0.635 (0.3840)	0.777 [-11.9, 0.999]	0.0211 (0.00529)	0.0203 [0.00812, 0.201]	30.3 (1.98)	30.3 [10.7, 38.8]
Modified Diffusion equation	-499 (6620)	0.814 [-613000, 0.996]	0.2370 (0.78500)	0.0200 [0.00348, 26.1]	324.4 (14.30)	30.5 [-30.5, 45.9]
Modified Poisson equation	-535 (7110)	0.741 [-668000, 0.997]	0.2330 (0.79700)	0.0213 [0.00519, 27.3]	23.8 (13.50)	29.8 [-31.1, 42.4]

In Appendix A, the mean and standard deviation of R-squared, RMSE, and SNR of the reconstructed signals individually from all subjects, for each dropout level repeated four times, are reported in Tables A.1 to A.4 for each method separately.

After marking 2% of the bad epochs for all subjects, the ratio of reconstructed epochs with an R-squared of more than 0.7 to the total reconstructed epochs is reported as a percentage in Table 3.

Another important criterion in recovering the lost signal is the time required for its implementation. Therefore, the average time required to implement each method to reconstruct a 500-millisecond epoch is shown in Table 4.

Table 3. The percentage of epochs with a R-squared greater than 70%

Method	Percentage (%)
Mean	97.0867
Median	99.3269
Trimmed mean	98.6557
Finite Element Method (FEM)	59.2862
Modified Diffusion equation	59.8412
Modified Poisson equation	52.8035

Table 4. The required average time to reconstruct an epoch

Method	Time (μs)
Mean	3.4396
Median	5.8683
Trimmed mean	9.5154
Finite Element Method (FEM)	2.8705
Modified Diffusion equation	581.5996
Modified Poisson equation	665.8979

4. Discussion

MEG signals exhibit strong spatial and temporal correlations due to neuronal activity. Adjacent channels often measure similar signals, which means that even when some channels are corrupted or lost, the remaining ones still hold valuable information. By leveraging these correlations, we can reconstruct the corrupted signals using the intact data. Research shows that no studies have been conducted to reconstruct low-quality or corrupted channel data for MEG signals. Therefore, the importance and innovation of this research are to recover and reconstruct the information on bad epochs to be used in diagnosis. In this study, six signal reconstruction methods were investigated to deal with the reduction of data elimination. While these reconstructions may not perfectly replicate the lost information, they provide statistically sound estimates. This is particularly important in biomedical contexts, where having a reliable estimate of brain activity is more

beneficial than having no data or discarding compromised channels.

As illustrated in Figure 2, the Mean, Median, and Trimmed Mean methods tend to smooth the reconstructed signal and reduce. The FEM method shows larger deviations from the original signal, suggesting that it may introduce additional distortions. The modified Diffusion and Poisson methods exhibit even greater discrepancies, indicating that they might not be as effective in preserving the original signal characteristics. These visual differences are matched with the results of Table 2, where the Mean, Median, and Trimmed Mean methods achieved higher R-squared and lower RMSE, indicating the best balance between signal preservation and noise reduction. In contrast, the FEM, Diffusion, and Poisson methods had lower R-squared and higher RMSE values.

The statistical tests demonstrated there is a significant direct and inverse coherence between R-squared with SNR and RMSE, respectively (P-value<0.001); therefore, to evaluate the introduced reconstruction methods' performance, one ought to examine the R-squared and also the smaller difference in signal amplitude of an epoch with the signal of neighboring epochs, the more accurate the reconstruction.

The results of statistical tests to investigate the performance of the analyzed methods were significantly dependent on Local Image Contrast (LIC), Average Nearest Neighbor (ANN), Percentage of the Outlier Border (POB), and missing rates up to 16% (P-value < 0.001). According to GLM test results, the Mean, Median, Trimmed mean, and FEM methods showed no significant differences in performance (P-value>0.05). However, these methods significantly outperformed modified Diffusion and Poisson methods with a high level of significance (P-value < 0.001).

On average, while repeating 4 times 2% selection of epochs, 97.09% for the Mean method, 99.33% for the Median method, and 98.65% for the Trimmed mean method had an R-squared greater than 0.70, indicating that the surface reconstruction methods are more efficient than other methods. Among these, the Trimmed Mean method demonstrated the highest reconstruction accuracy, achieving an average R-squared of 0.882 ± 0.0611 and an SNR of 33.8 ± 4.09, indicating that it effectively preserves the original structure of the signal while minimizing reconstruction errors. Besides, according to Table 2, the reconstruction error of the Mean, Median, Trimmed mean, and FEM methods has been acceptable, while on average, the Trimmed mean method achieves the lowest RMSE of 0.0155±0.00904. This suggests that it effectively preserves the original structure of the signal while minimizing reconstruction errors. The minimum average time required to reconstruct an epoch (reconstruction operation only) was 2.87 microseconds, achieved by the FEM Method. Afterward, the lowest average time for Mean, Median, and Trimmed mean methods with 3.4396, 5.8683, and 9.5154 microseconds was recorded, respectively.

While the Trimmed Mean method showed the highest reconstruction accuracy based on R-squared, SNR, and RMSE, it is important to acknowledge potential limitations. The effectiveness of this method may depend on the number and spatial distribution of available neighboring sensors. If too few intact sensors are present in a specific brain region, the reconstructed data might be less reliable. Furthermore, in clinical applications such as epilepsy monitoring, missing data in critical brain regions might impact diagnostic accuracy.

In general, increasing the number of sensors generally improves spatial resolution and enhances source localization accuracy. However, if the added sensors do not provide independent information (e.g., due to high correlation with nearby sensors), the reconstruction might introduce redundant or misleading data. This trade-off should be considered when designing MEG studies and selecting appropriate preprocessing methods.

The observed improvements in SNR and R-squared suggest that implementing reconstruction methods could reduce the need for discarding low-quality data, potentially lowering the cost of MEG data collection by minimizing sensor replacements and maintenance. Additionally, by improving the reliability of recorded signals, these methods may reduce the necessity for repeated scans in clinical and research settings, leading to more efficient data acquisition and analysis.

Although reconstruction methods significantly improve the quality of corrupted channels, their

effectiveness highly depends on the spatial distribution of available sensors. While this study did not include neural source localization techniques such as beamforming, likely, enhanced channel-level data quality could positively impact source estimation accuracy. Future research should systematically evaluate this effect by integrating reconstruction with source localization pipelines. Additionally, assessing the influence of reconstructed signals on downstream analyses—such as functional connectivity mapping and clinical diagnostics (e.g., epilepsy detection)—could provide valuable insights into the practical applications of these reconstruction methods.

5. Conclusion

This study compared various MEG signal reconstruction methods and demonstrated that surface-based approaches, particularly the Trimmed Mean method, provide the highest reconstruction accuracy. The results showed that preserving low-quality channels through interpolation can improve SNR and reduce reconstruction errors, which may ultimately benefit subsequent neural analyses. Overall, the Trimmed Mean method demonstrated the most balanced performance in terms of accuracy and robustness, making it a preferable choice for reconstructing missing MEG data. However, the Mean and Median methods also showed competitive results, while the FEM approach provided the fastest reconstruction time. In contrast, the modified Diffusion and Poisson methods exhibited significantly lower accuracy, suggesting that they may not be suitable for MEG signal reconstruction. However, the effectiveness of these methods depends on the spatial distribution of available sensors and the characteristics of missing data. While this study did not directly assess the impact of reconstruction on source localization, the observed improvements in signal quality suggest that future studies should investigate its potential role in enhancing source estimation accuracy. These findings highlight the importance of developing robust data reconstruction techniques to maximize the utility of MEG recordings in both research and clinical applications.

Acknowledgment

The authors would like to thank the University of Isfahan (UI) and the Avicenna Center of Excellence (ACE) for their support.

References

1- Sheng H. Wang, Muriel Lobier, Felix Siebenhühner, Tuomas Puoliväli, Satu Palva, and J. Matias Palva, "Hyperedge bundling: A practical solution to spurious interactions in MEG/EEG source connectivity analyses." *NeuroImage,* Vol. 173pp. 610-22, 2018/06/01/ (2018).

2- Luke Tait, Ayşegül Özkan, Maciej J Szul, and Jiaxiang Zhang, "A systematic evaluation of source reconstruction of resting MEG of the human brain with a new high-resolution atlas: Performance, precision, and parcellation." *Human Brain Mapping,* Vol. 42 (No. 14), pp. 4685-707, (2021).

3- J. M. Lina, R. Chowdhury, E. Lemay, E. Kobayashi, and C. Grova, "Wavelet-Based Localization of Oscillatory Sources From Magnetoencephalography Data." *IEEE Transactions on Biomedical Engineering,* Vol. 61 (No. 8), pp. 2350-64, (2014).

4- Matthew J. Brookes, Mark W. Woolrich, and Darren Price, "An Introduction to MEG Connectivity Measurements." in *Magnetoencephalography: From Signals to Dynamic Cortical Networks*, Selma Supek and Cheryl J. Aine, Eds. Cham: *Springer International Publishing*, (2019), pp. 433-70.

5- J. Vrba and S. E. Robinson, "SQUID sensor array configurations for magnetoencephalography applications." *Superconductor Science and Technology,* Vol. 15 (No. 9), pp. R51-R89, (2002).

6- Masashi Sato, Okito Yamashita, Masa-aki Sato, and Yoichi Miyawaki, "Information spreading by a combination of MEG source estimation and multivariate pattern classification." *PloS one,* Vol. 13 (No. 6), p. e0198806, (2018).

7- Mithun Diwakar *et al.*, "Accurate reconstruction of temporal correlation for neuronal sources using the enhanced dual-core MEG beamformer." *NeuroImage,* Vol. 56 (No. 4), pp. 1918-28, (2011).

8- Adam P. Baker *et al.*, "Fast transient networks in spontaneous human brain activity." *Elife,* Vol. 3p. e01867, 2014/03/25 (2014).

9- Monica Garcia-Alloza and Brian J. Bacskai, "Techniques for brain imaging in vivo." *NeuroMolecular Medicine,* Vol. 6 (No. 1), pp. 65-78, 2004/08/01 (2004).

10- Matti S. Hämäläinen, "Magnetoencephalography: A tool for functional brain imaging." *Brain Topography,* Vol. 5 (No. 2), pp. 95-102, (1992).

11- Vinh Tan *et al.*, "Preliminary Observations of Resting-State Magnetoencephalography in Nonmedicated Children with Obsessive-Compulsive Disorder." *Journal*

of Child and Adolescent Psychopharmacology, Vol. 32 (No. 10), pp. 522-32, (2022).

12- Bhargava K. Gautham *et al.*, "Automated lateralization of temporal lobe epilepsy with cross frequency coupling using magnetoencephalography." *Biomedical Signal Processing and Control,* Vol. 72p. 103294, 2022/02/01/ (2022).

13- Víctor Rodríguez-González *et al.*, "Unveiling the alterations in the frequency-dependent connectivity structure of MEG signals in mild cognitive impairment and Alzheimer's disease." *Biomedical Signal Processing and Control,* Vol. 87p. 105512, 2024/01/01/ (2024).

14- Pinar Ozel, Ali Karaca, Ali Olamat, Aydin Akan, Mehmet Akif Ozcoban, and Oguz Tan, "Intrinsic synchronization analysis of brain activity in obsessive–compulsive disorders." *International Journal of Neural Systems,* Vol. 30 (No. 09), p. 2050046, (2020).

15- Dengxuan Bai, Wenpo Yao, Shuwang Wang, Wei Yan, and Jun Wang, "Recurrence network analysis of schizophrenia MEG under different stimulation states." *Biomedical Signal Processing and Control,* Vol. 80p. 104310, 2023/02/01/ (2023).

16- Jan-Mathijs Schoffelen and Joachim Gross, "Source connectivity analysis with MEG and EEG." *Human Brain Mapping,* Vol. 30 (No. 6), pp. 1857-65, (2009).

17- Zhenfeng Gao, Fuzhi Cao, Nan An, and Xiaolin Ning, "Automatic co-registration of OPM-MEG and MRI using a 3D laser scanner." *Measurement,* Vol. 223p. 113729, 2023/12/01/ (2023).

18- Alain de Cheveigné and Dorothée Arzounian, "Robust detrending, rereferencing, outlier detection, and inpainting for multichannel data." *NeuroImage,* Vol. 172pp. 903-12, (2018).

19- John G Samuelsson, Noam Peled, Fahimeh Mamashli, Jyrki Ahveninen, and Matti S Hämäläinen, "Spatial fidelity of MEG/EEG source estimates: A general evaluation approach." *NeuroImage,* Vol. 224p. 117430, (2021).

20- Joachim Gross *et al.*, "Good practice for conducting and reporting MEG research." *NeuroImage,* Vol. 65pp. 349-63, (2013).

21- Ruonan Wang, Zhihui Jia, Ruochen Zhao, Yang Gao, and Xiaolin Ning, "OPM-MEG bad channel identification method based on the improved box-isolation forest algorithm." *Measurement,* Vol. 224p. 113948, 2024/01/01/ (2024).

22- Mikko A Uusitalo and Risto J Ilmoniemi, "Signal-space projection method for separating MEG or EEG into components." *Medical and biological engineering and computing,* Vol. 35 (No. 2), pp. 135-40, (1997).

23- Andrea Mognon, Jorge Jovicich, Lorenzo Bruzzone, and Marco Buiatti, "ADJUST: An automatic EEG artifact detector based on the joint use of spatial and temporal features." *Psychophysiology,* Vol. 48 (No. 2), pp. 229-40, (2011).

24- Michel Besserve, Karim Jerbi, Francois Laurent, Sylvain Baillet, Jacques Martinerie, and Line Garnero, "Classification methods for ongoing EEG and MEG signals." *Biological research,* Vol. 40 (No. 4), pp. 415-37, (2007).

25- Keita Suzuki and Okito Yamashita, "MEG current source reconstruction using a meta-analysis fMRI prior." *NeuroImage,* Vol. 236p. 118034, (2021).

26- K. Sekihara, K. E. Hild, 2nd, and S. S. Nagarajan, "A novel adaptive beamformer for MEG source reconstruction effective when large background brain activities exist." *IEEE Trans Biomed Eng,* Vol. 53 (No. 9), pp. 1755-64, Sep (2006).

27- Matthew J. Brookes *et al.*, "Beamformer reconstruction of correlated sources using a modified source model." *NeuroImage,* Vol. 34 (No. 4), pp. 1454-65, (2007).

28- Alain de Cheveigné and Jonathan Simon, "Sensor Noise Suppression." *Journal of Neuroscience Methods,* Vol. 168pp. 195-202, (2008).

29- Makoto Fukushima, Okito Yamashita, Thomas R. Knösche, and Masa-aki Sato, "MEG source reconstruction based on identification of directed source interactions on whole-brain anatomical networks." *NeuroImage,* Vol. 105pp. 408-27, (2015).

30- Alain de Cheveigné, "Sparse time artifact removal." *Journal of Neuroscience Methods,* Vol. 262pp. 14-20, (2016).

31- Hanie Arabian, Alireza Karimian, and Hamid R Marateb, "Repair of Poor Signal of Magnetoencephalography Channel Data." *Frontiers in Biomedical Technologies,* Vol. 0 (No. 0), 05/10 (2024).

32- Carolina Migliorelli, Joan F Alonso, Sergio Romero, Rafał Nowak, Antonio Russi, and Miguel A Mañanas, "Automated detection of epileptic ripples in MEG using beamformer-based virtual sensors." *Journal of Neural Engineering,* Vol. 14 (No. 4), p. 046013, (2017).

33- F. Tadel, S. Baillet, J. C. Mosher, D. Pantazis, and R. M. Leahy, "Brainstorm: a user-friendly application for MEG/EEG analysis." (in eng), *Comput Intell Neurosci,* Vol. 2011p. 879716, (2011).

34- Robert Oostenveld, Pascal Fries, Eric Maris, and Jan-Mathijs Schoffelen, "FieldTrip: Open Source Software for Advanced Analysis of MEG, EEG, and Invasive Electrophysiological Data." Vol. 2011p. 156869, (2011).

35- Simon Little, James Bonaiuto, Sofie S. Meyer, Jose Lopez, Sven Bestmann, and Gareth Barnes, "Quantifying the performance of MEG source reconstruction using resting state data." *NeuroImage,* Vol. 181pp. 453-60, (2018).

36- P. Ghaderi and H. R. Marateb, "Muscle Activity Map Reconstruction from High Density Surface EMG Signals

With Missing Channels Using Image Inpainting and Surface Reconstruction Methods." *IEEE Transactions on Biomedical Engineering,* Vol. 64 (No. 7), pp. 1513-23, (2017).

37- Hamid R Marateb, Monica Rojas-Martinez, Marjan Mansourian, Roberto Merletti, and Miguel A Mananas Villanueva, "Outlier detection in high-density surface electromyographic signals." *Medical & biological engineering & computing,* Vol. 50pp. 79-89, (2012).

38- M. S. Hämäläinen and R. J. Ilmoniemi, "Interpreting magnetic fields of the brain: minimum norm estimates." (in eng), *Med Biol Eng Comput,* Vol. 32 (No. 1), pp. 35-42, Jan (1994).

39- S. Taulu, J. Simola, and M. Kajola, "Applications of the signal space separation method." *IEEE Transactions on Signal Processing,* Vol. 53 (No. 9), pp. 3359-72, (2005).

40- Jiwoon Lee and Cheolsoo Park, "Restoration of Time-Series Medical Data with Diffusion Model." in *2022 IEEE International Conference on Consumer Electronics-Asia (ICCE-Asia)*, (2022): *IEEE*, pp. 1-4.

41- A. J. Dobson, & Barnett, A., An Introduction to Generalized Linear Models. Fourth Edition ed. *CRC Press*, (2018).

42- Tuomas Vainio, Teemu Mäkelä, Sauli Savolainen, and Marko Kangasniemi, "Performance of a 3D convolutional neural network in the detection of hypoperfusion at CT pulmonary angiography in patients with chronic pulmonary embolism: a feasibility study." *European radiology experimental,* Vol. 5 (No. 1), pp. 1-12, (2021).

43- R Core Team. (2022). R: A language and environment for statistical computing. *R Foundation for Statistical Computing*, Vienna, Austria. [Online]. Available: https://www.R-project.org/.

44- I. C Marschner, " glm2: Fitting generalized linear models with convergence problems." *The R Journal,* Vol. 3(2), pp. 12-15, (2011).

.